diagnostics

MDPI

Article

Software-Assisted Subtraction with Ultrasound-Correlated Interpretation Reduces Interpretive Ambiguity in Parathyroid Scintigraphy: A Preliminary Prospective Reporting Study

Seckin Bilgic [1,*], Elif Isleyen Colak [1], Irem Koroglu [2], Degercan Yesilyurt [3], Kadircan Karatoprak [4], Ozen Oz Gul [4], Ercument Gurluler [3] and Eray Alper [1]

[1] Department of Nuclear Medicine, Medical Faculty, Bursa Uludag University, Bursa 16059, Turkey; elifisleyencolak@uludag.edu.tr (E.I.C.); ealper@uludag.edu.tr (E.A.)
[2] Department of Nuclear Medicine, Bursa Yuksek Ihtisas Training and Research Hospital, University of Health Sciences, Bursa 16310, Turkey; iremyavas24@gmail.com
[3] Department of General Surgery, Medical Faculty, Bursa Uludag University, Bursa 16059, Turkey; degercanyesilyurt@uludag.edu.tr (D.Y.); gurluler@gmail.com (E.G.)
[4] Department of Internal Medicine, Division of Endocrinology and Metabolic Diseases, Medical Faculty, Bursa Uludag University, Bursa 16059, Turkey; karatoprak.kadircan@gmail.com (K.K.); drozenoz@gmail.com (O.O.G.)
* Correspondence: seckinbilgic@uludag.edu.tr; Tel.: +90-(533)-473-25-69

Abstract

Background/Objectives: Parathyroid imaging is used for preoperative localization rather than biochemical diagnosis. Conventional planar and SPECT-based scintigraphy may yield equivocal reports when thyroid activity obscures lesion localization. This study evaluated whether combining software-assisted subtraction imaging with ultrasound-correlated interpretation improves reporting certainty and reduces ambiguity. **Methods**: This prospective reporting study included 96 consecutive patients referred for parathyroid scintigraphy because of biochemical or clinical suspicion of primary hyperparathyroidism. Each anonymized imaging dataset was evaluated by two independent consensus reader pairs using different interpretation strategies. The control arm (CTRL) used conventional dual-time-point Tc-99m sestamibi planar and SPECT images with Tc-99m pertechnetate thyroid images. The intervention arm (INT) additionally used software-assisted subtraction images and ultrasound-correlated interpretation. Endpoints included suspected parathyroid adenoma (PTA)-positive reporting, certainty, clinically actionable localization, high-confidence localization, and non-actionable reporting. Surgical/pathological reference localization was available in 22 operated patients. **Results**: INT increased PTA-positive reporting compared with CTRL [82/96 (85.4%) vs. 53/96 (55.2%), $p < 0.001$]. Median certainty increased from 1 (IQR, 0–2) to 3 (IQR, 1–3) ($p < 0.001$). Clinically actionable localization increased from 32/96 (33.3%) to 68/96 (70.8%) ($p < 0.001$), and high-confidence localization increased from 17/96 (17.7%) to 55/96 (57.3%) ($p < 0.001$). Non-actionable reporting decreased from 64/96 (66.7%) to 28/96 (29.2%). In the operated subgroup, correct localization was higher with INT [20/22 (90.9%) vs. 12/22 (54.5%), $p = 0.008$]. **Conclusions**: Software-assisted subtraction imaging, when combined with ultrasound-correlated interpretation, improved the clinical usability of conventional parathyroid scintigraphy by increasing reporting certainty, reducing ambiguity, and improving actionable localization. Reference-based findings were supportive, and ongoing follow-up is expected to provide surgical/pathological confirmation for robust diagnostic accuracy analyses.

Check for updates

Academic Editor: Milan D. Jovanović

Received: 21 June 2026
Revised: 19 July 2026
Accepted: 24 July 2026
Published: 28 July 2026

Copyright: © 2026 by the authors. Licensee MDPI, Basel, Switzerland. This article is an open access article distributed under the terms and conditions of the Creative Commons Attribution (CC BY) license.

Keywords: parathyroid scintigraphy; subtraction imaging; Tc-99m sestamibi; ultrasound-correlated interpretation; diagnostic confidence; interpretive ambiguity

1. Introduction

Primary hyperparathyroidism is diagnosed biochemically, whereas imaging is primarily used to localize hyperfunctioning parathyroid tissue and guide the surgical approach. Accurate preoperative localization facilitates focused or minimally invasive parathyroidectomy and may reduce the extent of surgical exploration [1]. In recent years, parathyroid imaging has increasingly shifted toward PET/CT-based approaches. F-18 fluorocholine PET/CT has demonstrated superior diagnostic performance and lesion localization compared with cervical ultrasonography and Tc-99m sestamibi-based scintigraphic methods, including in patients with negative, equivocal, or discordant conventional imaging [2,3]. More recently, novel PET tracers, such as Ga-68 Trivehexin, have also shown promising lesion detection rates and have further emphasized the potential role of PET/CT in the localization of hyperfunctioning parathyroid tissue [4].

However, despite these promising results, PET/CT-based parathyroid imaging is not uniformly available in routine clinical practice. F-18 fluorocholine PET/CT requires PET/CT infrastructure, radiopharmaceutical availability, regulatory approval, and reimbursement coverage. Although recent data support its diagnostic superiority and possible workflow advantages, the broader implementation of F-18 fluorocholine PET/CT may still be limited by higher cost, local availability, reimbursement issues, and off-label or licensing considerations [3,5,6]. Although F-18 fluorocholine PET/CT currently provides the highest diagnostic performance, cervical ultrasonography and Tc-99m sestamibi scintigraphy remain among the most available and commonly used localization modalities in clinical practice, while the cost and limited availability of PET imaging may restrict its widespread first-line implementation [1].

Another important practical issue is the availability of hybrid SPECT/CT. SPECT/CT improves anatomical localization compared with planar or stand-alone SPECT imaging, and current guidelines recommend at least one SPECT(/CT) acquisition whenever possible [6]. However, in centers where conventional SPECT is available but SPECT/CT is not, anatomical correlation must often rely on high-resolution cervical ultrasonography. Cervical ultrasonography is a widely available, low-cost, and non-invasive modality that provides detailed anatomical assessment of the thyroid bed and surrounding cervical structures. Nevertheless, its diagnostic performance is operator-dependent and may be reduced in the presence of ectopic glands, concomitant nodular thyroid disease, previous neck surgery, multiglandular disease, or small lesions [7]. Parathyroid lesions may also be difficult to distinguish from thyroid nodules, cervical lymph nodes, or other perithyroidal structures because of overlapping morphological features [7,8]. Thyroid nodules may retain sestamibi in a pattern similar to that of parathyroid adenomas, making complementary thyroid imaging and anatomical correlation important for avoiding equivocal or false-positive interpretations [9]. Accordingly, ultrasonography may be most valuable when used as a complementary anatomical tool rather than as a stand-alone localization method. Correlation of scintigraphic findings with ultrasonographic morphology and vascular patterns may improve lesion characterization, clarify the relationship of a suspected focus to the thyroid gland, and reduce uncertainty in anatomically equivocal cases [7,10].

The performance of sestamibi-based parathyroid imaging is influenced not only by the imaging modality itself, but also by protocol selection, reader expertise, the use of dual-tracer or dual-phase strategies, and correlation with complementary anatomical

imaging. The wide variation in reported performance across centers therefore suggests that optimization of conventional workflows remains clinically relevant even in the PET/CT era [9].

The increasing availability of PET/CT-based alternatives may have unintentionally reduced attention to optimization of conventional sestamibi-based workflows. Subtraction imaging has long been proposed to improve the distinction of parathyroid activity from adjacent thyroid tissue, while targeted high-resolution ultrasonography may increase confidence when scintigraphic findings are equivocal [11]. More recent studies have further shown that dual-tracer subtraction protocols and combined ultrasonography–sestamibi approaches can improve lesion localization and diagnostic performance in primary hyperparathyroidism [10,12,13]. This raised a practical clinical question in our department: whether systematic use of these additional tools still provides meaningful interpretive value in the current PET/CT era.

Therefore, this prospective consensus reader-comparison study evaluated whether adding software-assisted subtraction and ultrasound-correlated interpretation to conventional parathyroid scintigraphy improved reporting certainty, reduced interpretive ambiguity, and increased clinically actionable localization. To our knowledge, this is the first prospective reporting study to assess the incremental value of this combined approach primarily in terms of reporting certainty, interpretive ambiguity, and clinically actionable localization rather than classical diagnostic accuracy.

2. Materials and Methods

2.1. Study Design and Patient Cohort

This was a prospective, blinded, two-group consensus-reader comparison study designed to evaluate the incremental contribution of software-assisted subtraction imaging, combined with ultrasound-correlated interpretation, in parathyroid scintigraphy. The primary focus of the study was not definitive diagnostic accuracy, but the effect of the additional interpretation strategy on reporting confidence, interpretive certainty, and ambiguity reduction.

Consecutive patients referred for parathyroid imaging because of biochemical or clinical suspicion of primary hyperparathyroidism between March 2025 and April 2026 were considered for inclusion. Each patient underwent routine dual-tracer parathyroid scintigraphy, including Tc-99m pertechnetate thyroid imaging and dual-time-point Tc-99m sestamibi parathyroid imaging. Clinical and biochemical parameters, including serum calcium, corrected calcium, phosphorus, parathyroid hormone, and vitamin D levels, were recorded when available. Genetic testing for multiple endocrine neoplasia type 1 (MEN1) was not performed as part of the study protocol, and MEN1 mutation status was not systematically available for the study cohort.

All datasets were anonymized before interpretation. Patient identifiers were removed, and the imaging studies were evaluated at the protocol level as observations.

2.2. Reporting Arms and Blinding

The study compared two interpretation strategies applied to the same patient cohort. The imaging studies were evaluated by four nuclear medicine physicians, who were divided into two independent consensus reader groups.

The control reporting arm consisted of two nuclear medicine physicians who interpreted the cases together using only the conventional imaging dataset, including dual-time-point Tc-99m sestamibi planar and SPECT images together with Tc-99m pertechnetate thyroid images. This group did not have access to software-assisted subtraction images or ultrasound-correlated findings.

In routine departmental practice, the Tc-99m pertechnetate image was reviewed visually to delineate thyroid tissue, whereas formal software-assisted registration, normalization, and digital subtraction were not performed systematically in every case. Accordingly, the CTRL arm was designed to reflect this conventional interpretation workflow.

The intervention reporting arm consisted of two nuclear medicine physicians who interpreted the same cases together using the full imaging dataset. This included the conventional scintigraphic images, software-assisted subtraction images, and available neck ultrasonography findings. In this arm, subtraction findings were evaluated together with ultrasound correlation to support anatomical localization and lesion characterization.

The two consensus reader pairs were independent of each other and were blinded to the other pair's interpretations and to final reference information during the reporting phase. Although the reader pairs were independent, the CTRL and INT observations were matched at the patient level because both interpretation strategies were applied to the same anonymized cases. Accordingly, comparisons between CTRL and INT were analyzed using paired statistical methods.

2.3. Image Acquisition Protocol

2.3.1. Planar Scintigraphy and Subtraction Imaging

Parathyroid scintigraphy was performed using a GE MEDICAL SYSTEMS Tandem Discovery 630 gamma camera (GE HealthCare, Waukesha, WI, USA). Patients were imaged in the head-first supine position, and planar images were acquired over the neck and upper mediastinum.

The planar protocol included a Tc-99m pertechnetate thyroid image acquired at 5 min, followed by Tc-99m sestamibi planar imaging at 20 min and 120 min. Planar images were acquired using a Tc-99m energy window of 126.45–154.55 keV and a 256 × 256 matrix. The Tc-99m pertechnetate thyroid image was used for thyroid background assessment and for software-assisted subtraction from the sestamibi dataset.

Software-assisted subtraction was performed on an Xeleris™ 4 DR nuclear medicine workstation (GE HealthCare, Milwaukee, WI, USA). The 5-min Tc-99m pertechnetate thyroid planar image and the early 20-min Tc-99m sestamibi planar image were loaded into the same processing workflow. Because both images were acquired in the anterior projection using the same matrix and acquisition geometry, their spatial correspondence was initially assessed visually. Image alignment was adjusted when necessary using the thyroid contours and adjacent anatomical landmarks. The pertechnetate image was subsequently scaled to approximate the thyroidal count distribution on the sestamibi image and subtracted from the sestamibi dataset. Image alignment and scaling were visually verified and, when necessary, conservatively adjusted to minimize residual thyroid activity while avoiding evident over-subtraction artifacts. The resulting subtraction images were interpreted in conjunction with the original pertechnetate, sestamibi planar, and SPECT images and were not used as stand-alone diagnostic images.

2.3.2. SPECT Acquisition

Early and delayed Tc-99m sestamibi SPECT acquisitions were obtained over the neck region after the 20-min and 120-min planar images, respectively. Each SPECT acquisition required approximately 10 min and was performed using the same gamma camera (GE HealthCare, Waukesha, WI, USA) system with a low-energy, high-resolution parallel-hole collimator. Tomographic acquisition was performed using a 128 × 128 matrix with a pixel spacing of approximately 4.42 × 4.42 mm. A step-and-shoot acquisition was performed over a 180° clockwise arc, starting at 270°, with 30 projections, an angular step of 6°, and

10 s per projection. The DICOM metadata indicated correction for center of rotation, energy, and uniformity.

2.3.3. Ultrasound Correlation

Neck ultrasonography correlation was performed using a LOGIQ P5 ultrasound system (GE Healthcare, Milwaukee, WI, USA) with an 8L linear probe. The probe bandwidth was 4–12 MHz. The Doppler function was not activated on the available ultrasound unit; therefore, color or power Doppler assessment was not performed. Ultrasound correlation was performed by a nuclear medicine physician/operator with 10 years of experience in neck ultrasonography and parathyroid imaging correlation.

In the intervention arm, ultrasound data were used as a supportive anatomical correlate for the scintigraphic findings. The correlated parameters included lesion side, pole-level localization, thyroidal or extrathyroidal relationship, mediastinal extension when present, and sonographic lesion size when identifiable. Ultrasound findings were not used as an independent reference standard for diagnostic accuracy; rather, they were incorporated into the intervention interpretation strategy to determine whether multimodal correlation improved reader confidence and reduced interpretive ambiguity.

2.4. Image Interpretation and Recorded Variables

For each reporting arm, the readers recorded the presence or absence of a suspected parathyroid adenoma. When a suspicious lesion was identified, anatomical localization was coded using predefined categories, including right upper pole, right middle pole, right lower pole, left upper pole, left middle pole, left lower pole, lateral location, isthmic location, intrathyroidal location, and mediastinal location.

A confidence-based diagnostic score was assigned for each positive interpretation using a three-tiered system:

- A score of 1 indicated findings suggestive of parathyroid adenoma.
- A score of 2 indicated findings most likely representing parathyroid adenoma.
- A score of 3 indicated findings highly consistent with parathyroid adenoma.

Negative cases were coded separately as no suspicious lesion. Negative reports were assigned a value of 0 for quantitative analyses. The PTA-Certainty Index was therefore defined as 0 for negative reports and 1–3 for suspected parathyroid adenoma-positive reports, according to the assigned confidence score. Clinically actionable localization was defined as suspected parathyroid adenoma positivity with a certainty score ≥ 2, whereas high-confidence localization was defined as suspected parathyroid adenoma positivity with a certainty score of 3. Non-actionable reporting was defined as either suspected parathyroid adenoma negativity or suspected parathyroid adenoma positivity with low certainty. This scoring system was used to quantify the level of interpretive certainty rather than to define histopathological truth. Therefore, upward movement in the confidence category between the control and intervention arms was interpreted as increased reporting confidence, whereas persistence in low-confidence or discordant categories was interpreted as residual ambiguity.

2.5. Reference Information and Exploratory Validation

Surgical and histopathological findings were recorded when available. At the time of data cutoff, 22 patients had undergone parathyroidectomy following routine clinical evaluation and therefore had surgical/pathological reference localization. Among patients without surgical reference, some were still awaiting surgery, whereas others had decided not to proceed with surgery after clinical evaluation. Thus, the availability of surgical reference reflected the timing of surgery and patient preference at the time of analysis.

Because surgical confirmation was available only in this subset, the study was not designed as a definitive diagnostic accuracy study. Accordingly, full patient-level diagnostic accuracy metrics requiring both reference-positive and reference-negative patients, such as patient-level specificity, negative predictive value, Youden index, and classical disease-detection AUC, were not used as primary endpoints.

For non-operated cases, concordant clinical, biochemical, scintigraphic, ultrasonographic, and follow-up information was recorded as supportive reference information when available. These data were used for exploratory interpretation and descriptive validation, particularly for cases with intervention-only positive findings or discordant localization between reporting arms.

Operated patients with histopathological confirmation were analyzed descriptively as a validation subset. This subset was used to contextualize the reporting findings but not to redefine the primary study objective.

2.6. Outcomes

The primary outcome was the paired difference in diagnostic confidence between the control and intervention reporting arms. The main analysis focused on whether software-assisted subtraction with ultrasound-correlated interpretation increased the certainty of reporting compared with conventional interpretation.

Secondary outcomes included the paired difference in PTA-positive reporting rate, reduction in low-confidence or ambiguous interpretations, intervention-only positive findings, control-only positive findings, localization-level discordance, and concordance between the two reporting approaches.

Additional exploratory outcomes included descriptive a comparison of operated and non-operated cases, concordance of reported lesion localization with surgical or histopathological findings when available, and the distribution of confidence-score transitions between the two reporting arms.

2.7. Statistical Analyses

All statistical analyses were performed using R statistical software version 4.6.0. Data import, cleaning, and preprocessing were performed using the readxl, dplyr, tidyr, stringr, janitor, and purrr packages. Descriptive summaries were generated using base R and tidyverse-based functions.

Paired categorical comparisons between the control and intervention reporting arms were performed using McNemar's test when appropriate. Agreement between reporting approaches was assessed using Cohen's kappa with the irr package (version 0.85). Ordinal paired variables, including diagnostic confidence scores, were compared using paired non-parametric tests. Confidence-score transitions were summarized using transition matrices to demonstrate the direction and magnitude of changes in interpretive certainty.

Cases were also categorized according to the direction of confidence change between the two reporting arms: increased confidence, unchanged confidence, decreased confidence, intervention-only positive interpretation, and control-only positive interpretation. These categories were used to evaluate whether the intervention strategy reduced interpretive ambiguity at the patient/protocol level. Lesion-location distributions were summarized descriptively according to INT localization, which provided the most complete anatomical categorization across the paired cohort. Because the location indicators were not mutually exclusive, particularly for lateral and intrathyroidal descriptors, each location category was analyzed separately. Exploratory associations between individual location indicators and clinical gain were evaluated using Fisher's exact test, with Benjamini–Hochberg correction for multiple comparisons. In an additional post hoc exploratory analysis, patients with an

isthmic, intrathyroidal, or mediastinal location were compared with the remaining cohort using Fisher's exact test.

Model outputs and test results were organized using the broom package. A two-sided p-value < 0.05 was considered statistically significant.

3. Results

The final study cohort included 96 patients with paired CTRL and INT readings (Figure 1). The median age was 58 years (IQR, 50.8–63.2), and 79 patients were female (82.3%). Median serum calcium was 10.5 mg/dL (IQR, 9.9–11.1), median corrected calcium was 10.0 mg/dL (IQR, 9.5–10.7), and median PTH was 167 pg/mL (IQR, 124.7–225.3). Median vitamin D level was 25.3 ng/mL (IQR, 18.8–35.1). On INT, median lesion dimensions 1, 2, and 3 were 8 mm (IQR, 7–11.2), 6 mm (IQR, 4–8), and 7 mm (IQR, 5.5–9.8), respectively. Surgical/pathological reference localization was available in 22 operated patients. Among the non-operated patients, some were awaiting surgery at the time of data cutoff, whereas others had elected not to proceed with the recommended operation. Baseline clinical, biochemical, and lesion-related characteristics are summarized in Table 1. A representative case illustrating the stepwise detection of a typical parathyroid adenoma with conventional sestamibi imaging, subtraction imaging, and ultrasound correlation is shown in Figure 2.

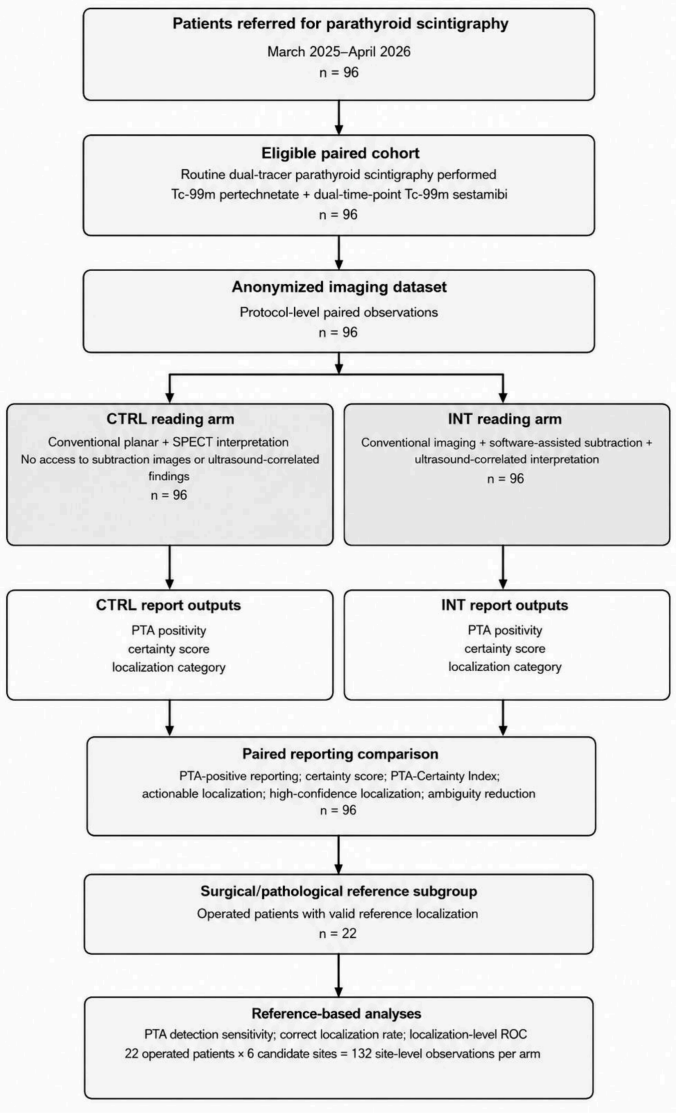


Figure 1. Study flow and reporting design.

Table 1. Baseline Demographic, Biochemical, and Imaging Characteristics of the Study Cohort.

Patients	**Available *n***	***n* = 96**
Age, years		
Median (IQR)		58 (50.8–63.2)
Sex,		
Female *n* (%)		79 (82.3%)
Calcium (mg/dL)	95	10.5 (9.9–11.1)
Corrected calcium (mg/dL)	62	10.0 (9.5–10.7)
Phosphorus (mg/dL)	79	2.8 (2.3–3.3)
PTH (pg/mL)	95	167 (124.7–225.3)
Vitamin D (ng/mL)	77	25.3 (18.8–35.1)
Calcium–PTH product	95	1707.4 (1274.0–2421.5)
Lesion size 1 (mm)	84	8 (7–11.2)
Lesion size 2 (mm)	83	6 (4–8)
Lesion size 3 (mm)	83	7 (5.5–9.8)
Estimated lesion volume (mm^3)	83	175.9 (80.6–438.8)
Operated patients		22/96 (22.9%)

Abbreviations: IQR, interquartile range; PTH, parathyroid hormone. Continuous variables are presented as median (IQR), and categorical variables as *n*/*N* (%). Available *n* indicates the number of patients with available data for each variable.

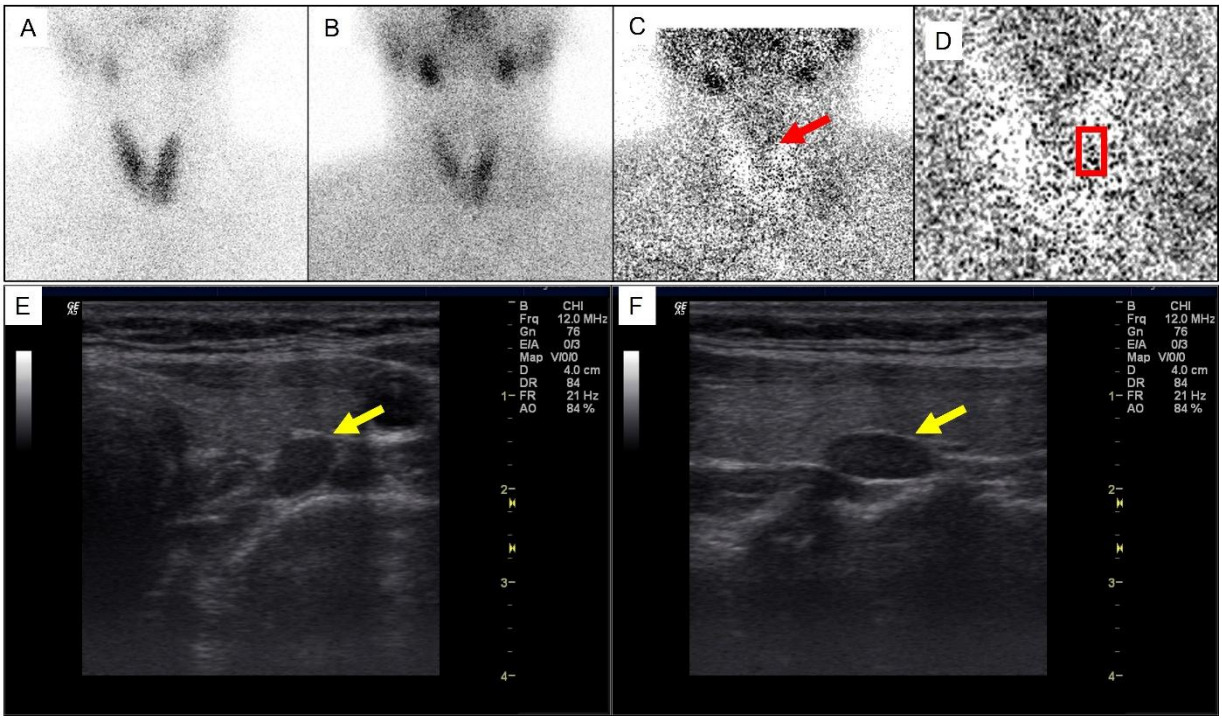


Figure 2. Representative case illustrating stepwise detection of a typical parathyroid adenoma using software-assisted subtraction and ultrasound correlation. (**A**) Early 20-min Tc-99m sestamibi planar image. (**B**) Delayed 120-min Tc-99m sestamibi planar image. (**C**) Full software-assisted subtraction image demonstrating a focal residual uptake suspicious for parathyroid adenoma (red arrow). (**D**) Magnified view of the subtraction focus shown in panel (**C**), with the focal area outlined by the red rectangle. Although the residual focus may appear broader on the full subtraction image, this visual impression is influenced by adjacent midline background activity and the limited spatial resolution of planar scintigraphy. (**E**) Axial ultrasound image showing a corresponding hypoechoic extrathyroidal lesion (yellow arrow). (**F**) Craniocaudal ultrasound image showing the same lesion (yellow arrow). This case illustrates how subtraction imaging and ultrasound correlation can improve lesion conspicuity, anatomical localization, and reporting confidence. The apparent extent of the subtraction focus should not be interpreted as a direct anatomical measurement of lesion size.

3.1. Paired Comparison of Reporting Certainty and Localization Endpoints

INT yielded a higher PTA-positive reporting rate than CTRL. A PTA-positive report was issued in 82/96 patients (85.4%) with INT and in 53/96 patients (55.2%) with CTRL ($p < 0.001$). Reporting certainty was also higher with INT, with a median certainty score of 3 (IQR, 1–3) compared with 1 (IQR, 0–2) for CTRL ($p < 0.001$). Similarly, the PTA-Certainty Index increased from a median of 1 (IQR, 0–2) with CTRL to 3 (IQR, 1–3) with INT ($p < 0.001$).

Clinically actionable localization was achieved in 68/96 patients (70.8%) with INT and in 32/96 patients (33.3%) with CTRL ($p < 0.001$). High-confidence localization was achieved in 55/96 patients (57.3%) with INT, compared with 17/96 patients (17.7%) with CTRL ($p < 0.001$). Paired reporting outcomes are summarized in Table 2.

Table 2. Paired comparison of reporting certainty and clinically actionable localization.

Endpoint	INT	CTRL	*p*-Value
PTA-positive report	82/96 (85.4%)	53/96 (55.2%)	<0.001 †
Certainty score, median (IQR)	3 (1–3)	1 (0–2)	<0.001 ‡
PTA-Certainty Index, median (IQR)	3 (1–3)	1 (0–2)	<0.001 ‡
Actionable localization	68/96 (70.8%)	32/96 (33.3%)	<0.001 †
High-confidence localization	55/96 (57.3%)	17/96 (17.7%)	<0.001 †

Abbreviations: CTRL, control reading based on standard interpretation; INT, intervention reading based on subtraction imaging with ultrasonographic correlation; IQR, interquartile range; PTA, parathyroid adenoma. Values are presented as *n*/*N* (%) unless otherwise indicated. All analyses were performed in 96 paired observations. The PTA-Certainty Index was calculated as PTA positivity multiplied by the certainty score, yielding a patient-level score from 0 to 3. Actionable localization was defined as PTA positivity with certainty ≥ 2. High-confidence localization was defined as PTA positivity with certainty = 3. † Exact McNemar/binomial test was used for paired binary outcomes. ‡ Wilcoxon signed-rank test was used for paired ordinal or index-based comparisons. *p*-values < 0.001 are shown as <0.001.

3.2. Reduction in Interpretive Ambiguity and Clinical Gain

When non-actionable reporting was defined as either PTA negativity or PTA positivity with low certainty, CTRL yielded non-actionable reports in 64/96 patients (66.7%), whereas INT yielded non-actionable reports in 28/96 patients (29.2%). This corresponded to an absolute reduction of 37.5 percentage points and a relative reduction of 56.2% in non-actionable reporting with INT.

In paired transition analysis, 35 patients changed from CTRL-negative to INT-positive, whereas 6 patients converted from CTRL-positive to INT-negative. For actionable localization, 41 patients gained actionability with INT, while 5 patients lost actionability (Figure 3). Similarly, high-confidence localization was gained in 41 patients and lost in 3 patients after INT.

Certainty scores increased with INT in 56/96 paired reports (58.3%), remained unchanged in 30/96 reports (31.2%), and decreased in 10/96 reports (10.4%) (Figure 4; Supplementary Figure S1). Among patients with a CTRL certainty score of 0, 29/43 patients shifted to an INT certainty score of 2 or 3, including 21 patients who shifted directly to an INT certainty score of 3. Overall, 41/96 patients (42.7%) fulfilled the predefined clinical gain criterion, defined as a negative or low-certainty CTRL result followed by INT PTA-positive localization with certainty ≥ 2. Two representative clinically gained cases are shown in Figures 5 and 6. In the first case, the lesion was not identified on CTRL interpretation, whereas INT enabled detection of a subtle focal uptake that was anatomically correlated with ultrasound and subsequently confirmed by surgical/pathological findings (Figure 5). In the second case, a small lesion that remained subtle on conventional scintigraphy became more conspicuous on software-assisted subtraction imaging and was anatomically corroborated by ultrasound, supporting confident PTA localization (Figure 6). A complementary CTRL-positive/INT-negative case is shown in Figure 7. In this patient,

a MIBI-avid thyroid nodule was classified as a high-confidence PTA by CTRL (certainty score of 3), whereas ultrasound-correlated interpretation demonstrated that the uptake corresponded to an intrathyroidal thyroid nodule, allowing INT to avoid a false-positive PTA interpretation.

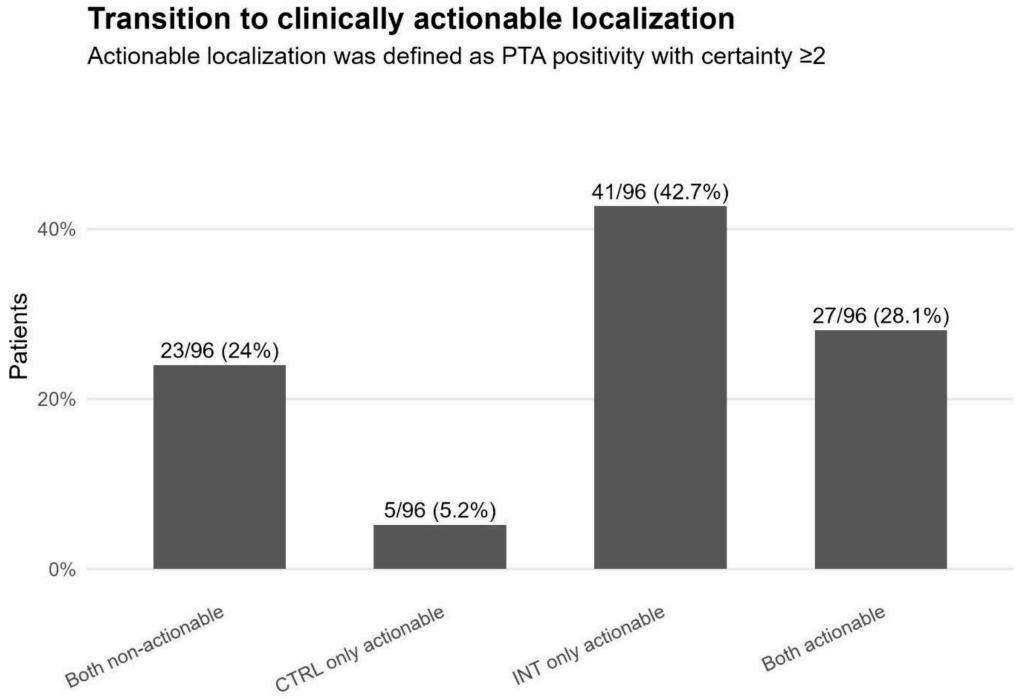


Figure 3. Transition to clinically actionable localization between CTRL and INT readings. Actionable localization was defined as PTA positivity with a certainty score ≥ 2. INT-only actionable cases represent patients who were non-actionable on CTRL reading but became clinically actionable after software-assisted subtraction with ultrasound-correlated interpretation.

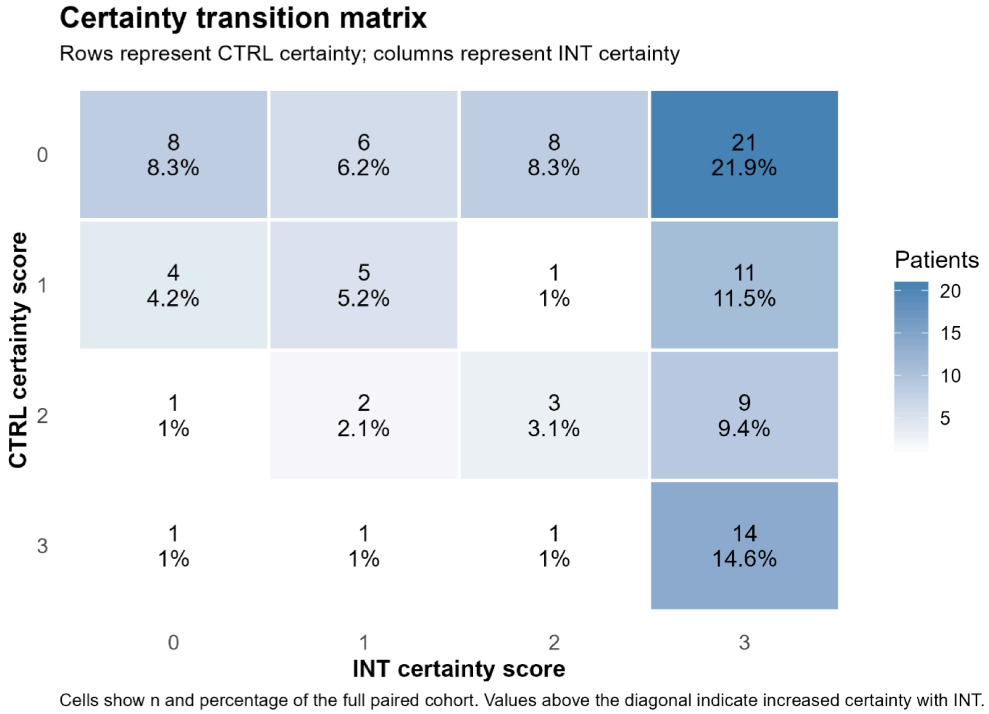


Figure 4. Patient-level transition matrix of reporting certainty from CTRL to INT interpretation. Rows represent CTRL certainty scores, and columns represent INT certainty scores. Certainty was coded as 0 for a negative report, 1 for findings suggestive of parathyroid adenoma, 2 for findings most likely

representing parathyroid adenoma, and 3 for findings highly consistent with parathyroid adenoma. Each cell shows the number of patients and the corresponding percentage of the entire cohort (n = 96) with that specific CTRL-to-INT transition. Transitions in which the INT score exceeded the CTRL score indicate increased certainty, identical scores indicate unchanged certainty, and transitions in which the INT score was lower than the CTRL score indicate decreased certainty. Overall, certainty increased in 56/96 patients (58.3%), remained unchanged in 30/96 (31.2%), and decreased in 10/96 (10.4%).

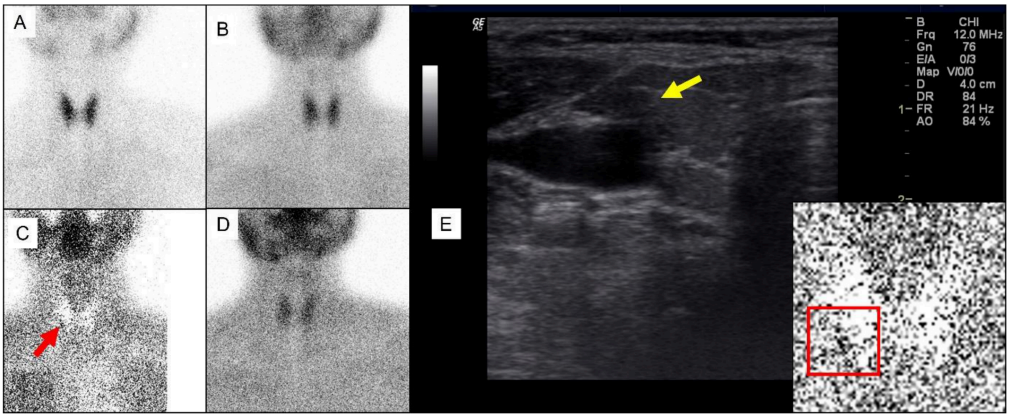


Figure 5. Representative clinically gained case illustrating detection of a small parathyroid adenoma with software-assisted subtraction and ultrasound-correlated interpretation. (**A**) Five-minute Tc-99m pertechnetate thyroid planar image. (**B**) Early 20-min Tc-99m sestamibi planar image. (**C**) Software-assisted subtraction image demonstrating subtle focal residual uptake suspicious for parathyroid adenoma (red arrow). (**D**) Delayed 120-min Tc-99m sestamibi planar image. (**E**) Ultrasound image showing a corresponding ovoid cervical lesion at the same anatomical location; the inset represents a magnified view of the focal residual uptake shown in panel (yellow arrow) (**C**). The lesion was not identified on CTRL interpretation, whereas INT enabled detection of the subtle scintigraphic focus. Because of its ovoid morphology, the lesion had initially been interpreted as a lymph node on ultrasound; however, subsequent surgical and histopathological findings confirmed a parathyroid adenoma at this location.

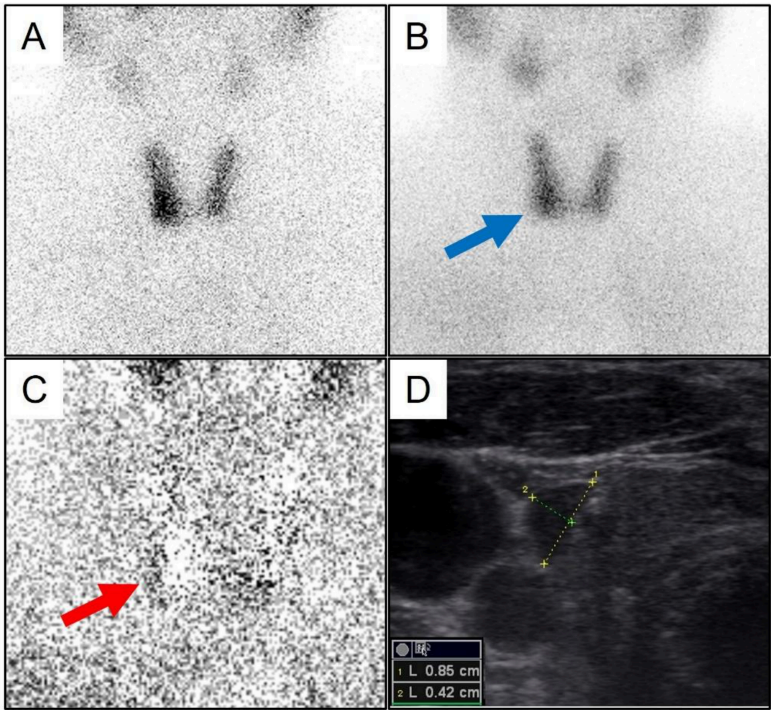


Figure 6. Representative case illustrating improved localization of a small parathyroid lesion using software-assisted subtraction and ultrasound-correlated interpretation. (**A**) Five-minute Tc-99m

pertechnetate thyroid planar image. (**B**) Early 20-min Tc-99m sestamibi planar image showing a subtle focal uptake adjacent to the thyroid gland (blue arrow). (**C**) Software-assisted subtraction image demonstrating more conspicuous focal residual uptake suspicious for a parathyroid adenoma (red arrow). (**D**) Ultrasound image showing a corresponding small hypoechoic lesion at the same anatomical location. This case illustrates the complementary value of subtraction imaging and ultrasound correlation in improving the conspicuity and confident localization of a small parathyroid lesion.

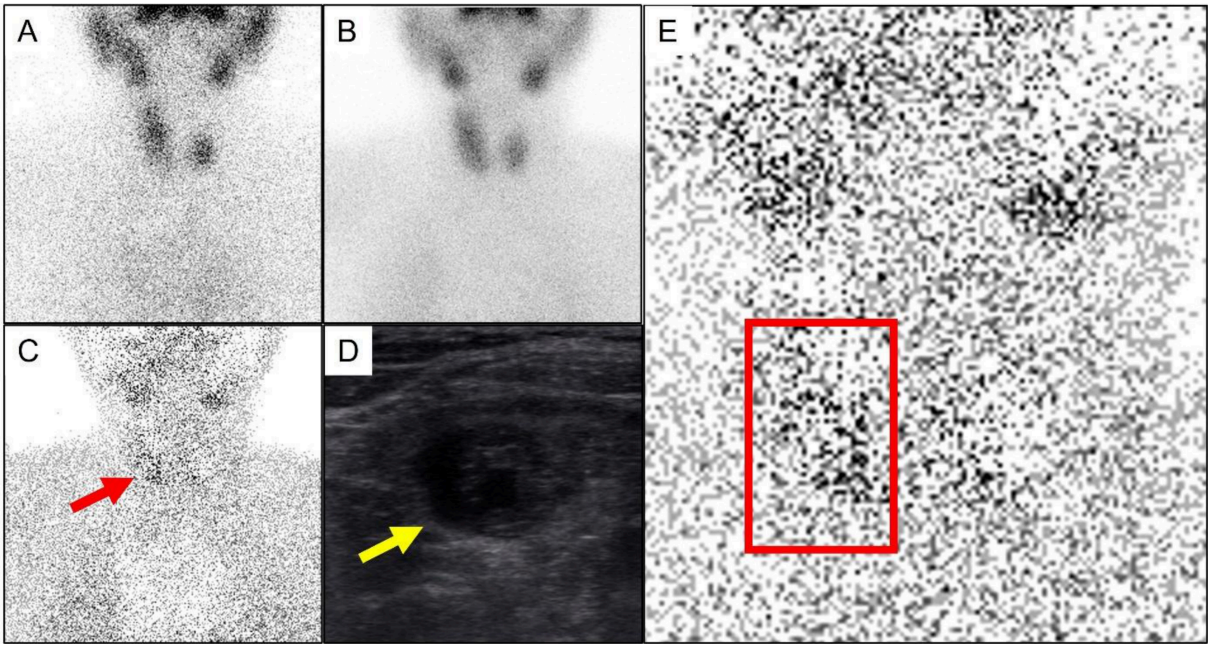


Figure 7. Representative case illustrating avoidance of overcalling a MIBI-avid thyroid nodule as a parathyroid adenoma through ultrasound-correlated interpretation. (**A**) Five-minute Tc-99m pertechnetate thyroid planar image. (**B**) Early 20-min Tc-99m sestamibi planar image showing focal uptake in the thyroid region. (**C**) Software-assisted subtraction image demonstrating focal residual uptake (red arrow). (**D**) Ultrasound image demonstrating that the corresponding lesion was an intrathyroidal thyroid nodule (yellow arrow). (**E**) Magnified view of the subtraction focus shown in panel (**C**), with the region of interest outlined by the red rectangle. The focus was classified as a high-confidence PTA by CTRL (certainty score of 3), whereas ultrasound correlation in INT supported its thyroidal origin and helped avoid overcalling it as a parathyroid lesion.

3.3. PTH-Stratified Analysis

The advantage of INT over CTRL was observed across PTH strata. In patients with PTH 80–119 pg/mL, actionable localization was achieved in 7/16 patients (43.8%) with INT compared with 1/16 patient (6.2%) with CTRL. In patients with PTH 120–159 pg/mL, actionable localization was 16/24 (66.7%) with INT and 6/24 (25.0%) with CTRL. In patients with PTH $\geq$ 160 pg/mL, actionable localization was 42/52 (80.8%) with INT and 24/52 (46.2%) with CTRL.

High-confidence localization showed a similar pattern across PTH strata. INT achieved high-confidence localization in 5/16 patients (31.2%) with PTH 80–119 pg/mL, 12/24 patients (50.0%) with PTH 120–159 pg/mL, and 35/52 patients (67.3%) with PTH $\geq$ 160 pg/mL. The corresponding CTRL rates were 1/16 (6.2%), 2/24 (8.3%), and 14/52 (26.9%), respectively. Clinical gain rates were broadly similar across the three main PTH strata: 7/16 (43.8%), 10/24 (41.7%), and 21/52 (40.4%), respectively. PTH-stratified outcomes are summarized in Table 3.

Table 3. PTH-stratified comparison of INT and CTRL reporting performance.

PTH Group, pg/mL	*n*	INT PTA Positive	CTRL PTA Positive	INT Actionable Localization	CTRL Actionable Localization	INT High-Confidence Localization	CTRL High-Confidence Localization
80–119	16	10/16 (62.5%)	5/16 (31.2%)	7/16 (43.8%)	1/16 (6.2%)	5/16 (31.2%)	1/16 (6.2%)
120–159	24	21/24 (87.5%)	10/24 (41.7%)	16/24 (66.7%)	6/24 (25.0%)	12/24 (50.0%)	2/24 (8.3%)
≥160	52	47/52 (90.4%)	36/52 (69.2%)	42/52 (80.8%)	24/52 (46.2%)	35/52 (67.3%)	14/52 (26.9%)

Abbreviations: Values are presented as *n*/*N* (%). PTH, parathyroid hormone; INT, intervention reading based on subtraction imaging with ultrasonographic correlation; CTRL, control reading based on standard interpretation; PTA, parathyroid adenoma. Actionable localization was defined as PTA positivity with a certainty score ≥ 2, and high-confidence localization as PTA positivity with a certainty score of 3. Patients with PTH < 80 pg/mL or missing PTH values were excluded from this subgroup analysis.

3.4. Surgical/Pathological Reference-Based Analysis

Among the 22 operated patients with valid surgical/pathological reference localization, PTA detection sensitivity was 21/22 (95.5%; 95% CI, 77.2–99.9%) for INT and 17/22 (77.3%; 95% CI, 54.6–92.2%) for CTRL. This difference did not reach statistical significance in paired analysis (exact McNemar $p = 0.219$). Correct localization rate was significantly higher with INT. INT correctly localized the reference-confirmed lesion in 20/22 patients (90.9%; 95% CI, 70.8–98.9%), whereas CTRL correctly localized the lesion in 12/22 patients (54.5%; 95% CI, 32.2–75.6%; exact McNemar $p = 0.008$). In the paired reference subgroup, INT was correct while CTRL was incorrect in 8 patients, whereas there were no patients in whom CTRL was correct and INT was incorrect.

Because the operated reference cohort consisted only of pathology-positive patients, patient-level specificity, negative predictive value, Youden index, and classical disease-detection AUC were not estimable. Reference-based operated subgroup findings are summarized in Table 4.

Table 4. Reference-based diagnostic and localization performance.

Endpoint	INT, *n*/*N* (%)	95% CI	CTRL, *n*/*N* (%)	95% CI	Exact McNemar *p*
PTA detection sensitivity	21/22 (95.5%)	77.2–99.9%	17/22 (77.3%)	54.6–92.2%	0.219
Correct localization rate	20/22 (90.9%)	70.8–98.9%	12/22 (54.5%)	32.2–75.6%	0.008

Abbreviations: CI, confidence interval; CTRL, control reading based on standard interpretation; INT, intervention reading based on subtraction imaging with ultrasonographic correlation; PTA, parathyroid adenoma. Values are presented as *n*/*N* (%), with exact binomial 95% confidence intervals. PTA detection sensitivity was defined as the proportion of reference-confirmed patients in whom a PTA-positive lesion was reported. Correct localization rate was defined as concordance between the reported lesion location and the surgical/pathological reference location. Patient-level specificity, NPV, Youden index, and classical disease-detection AUC were not estimable because the reference cohort consisted only of pathology-positive operated patients.

3.5. Localization-Level ROC Analysis in the Operated Subgroup

To further characterize reference-based localization performance, a localization-level analysis was performed only in the operated subgroup with surgical/pathological reference localization. Each operated patient was expanded into six candidate parathyroid sites, yielding 132 localization-level observations per reporting arm. For each patient, the surgically confirmed site was coded as positive, and the remaining five candidate sites were coded as negative.

In this localization-level analysis, INT showed higher sensitivity than CTRL (20/22, 90.9% vs. 12/22, 54.5%), while specificity remained high in both arms (109/110, 99.1% vs. 106/110, 96.4%). The corresponding PPV and NPV were 95.2% and 98.2% for INT, compared with 75.0% and 91.4% for CTRL. Overall localization-level accuracy was 97.7% for INT and 89.4% for CTRL.

For ROC visualization, binary localization predictions were displayed as operating points in ROC space rather than as full thresholded ROC curves (Figure 8A). The binary operating-point AUC, equivalent to balanced accuracy under a piecewise-linear connection, was 0.950 for INT and 0.755 for CTRL. In a certainty-weighted localization-level ROC analysis, using a score of 0 for unreported sites and the assigned certainty score for reported sites, INT achieved a higher AUC than CTRL (0.954; 95% CI, 0.892–1.000 vs. 0.756; 95% CI, 0.647–0.864) (Figure 8B). Cluster bootstrap analysis showed an AUC difference of 0.198 in favor of INT. These ROC findings should be interpreted as localization-level discrimination within the operated reference subgroup rather than patient-level disease-detection accuracy.

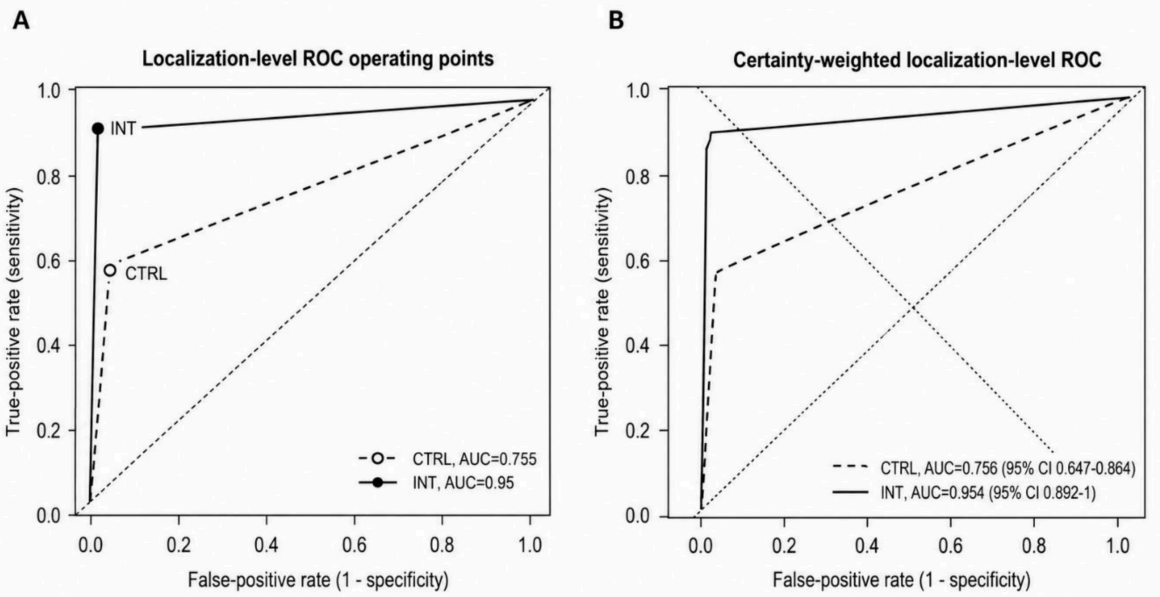


Figure 8. Localization-level ROC analysis in the operated subgroup. (**A**) Binary localization-level ROC operating points for CTRL and INT. Binary localization predictions provide one operating point per reporting arm rather than full thresholded ROC curves. (**B**) Certainty-weighted localization-level ROC curves using a score of 0 for unreported sites and the assigned certainty score for reported sites. These analyses were restricted to operated patients with surgical/pathological reference localization and should be interpreted as localization-level discrimination rather than patient-level disease-detection accuracy.

Based on INT interpretation, pole-level lesion locations included the right upper pole in 8 patients, the right middle pole in 9, the right lower pole in 32, the left upper pole in 4, the left middle pole in 7, and the left lower pole in 23. Additional anatomical descriptors included lateral location in 52 patients, intrathyroidal location in 7, isthmic location in 3, and mediastinal location in 2. Because these location indicators were not mutually exclusive, particularly for the lateral and intrathyroidal descriptors, the counts should not be summed to represent the total number of lesions. In exploratory analyses, no individual location indicator was significantly associated with clinical gain after Benjamini–Hochberg correction for multiple comparisons. Clinical gain also did not differ significantly between patients with an isthmic, intrathyroidal, or mediastinal location and the remaining cohort (Fisher exact $p = 0.754$). These analyses should be interpreted cautiously because of the small number of patients in several anatomical subgroups.

3.6. Exploratory Ultrasound-Related and Lesion Measurement Analyses

Ultrasound-related findings were associated with higher INT endpoint-positive rates. In patients with a recorded ultrasound finding, INT actionable localization was observed in 50/61 patients (82.0%), compared with 18/35 patients (51.4%) without a recorded ultra-

sound finding. Clinically gained status was also more frequent in patients with a recorded ultrasound finding than in those without one: 33/61 (54.1%) versus 8/35 (22.9%). Similar patterns were observed for typical ultrasound appearance, where INT actionable localization was 66/72 (91.7%) in patients with typical ultrasound appearance and 2/24 (8.3%) in those without typical ultrasound appearance. Because ultrasound information was incorporated into the INT interpretation workflow, these analyses were considered exploratory and descriptive rather than independent predictive analyses (Supplementary Figure S2).

Lesion measurement analyses were exploratory because lesion dimensions were derived from INT reports. Median lesion dimensions were comparable between patients with and without clinically actionable gain. In patients with clinically actionable gain, median lesion dimensions 1, 2, and 3 were 8 mm (IQR, 7–11), 6 mm (IQR, 5–7), and 7 mm (IQR, 6–8.5), respectively. In patients without clinically actionable gain, the corresponding values were 8 mm (IQR, 6–12), 6 mm (IQR, 3.25–8), and 7.25 mm (IQR, 5–10.5), respectively. Estimated lesion volume in mm^3 was also similar between groups (Supplementary Figure S3). These findings suggest that the clinical benefit of INT was not simply attributable to larger lesion dimensions.

4. Discussion

In this prospective reporting study, software-assisted subtraction imaging, combined with ultrasound-correlated interpretation, substantially improved the clinical usability of parathyroid scintigraphy reports. Compared with conventional planar and SPECT-based interpretation, the intervention strategy increased PTA-positive reporting, shifted certainty scores upward, and markedly increased both clinically actionable and high-confidence localization. Because the same anonymized imaging datasets were evaluated under two reporting conditions, these differences are unlikely to reflect cohort-level variation and more directly reflect the incremental contribution of the interpretation strategy.

The most clinically relevant finding was the reduction in non-actionable or ambiguous reporting. In routine practice, a negative or weakly suggestive report may be insufficient for focused operative planning, even when biochemical primary hyperparathyroidism is established. The predefined actionable localization endpoint was therefore designed to capture whether the report provided a localization statement potentially useful for clinical decision-making, rather than simply whether any abnormal uptake was described. This distinction is important because imaging in primary hyperparathyroidism is intended to localize hyperfunctioning parathyroid tissue before surgery, not to establish the biochemical diagnosis [6,9,14].

The paired transition analyses further support this interpretation. More than half of the reports showed increased certainty after the intervention strategy, whereas decreased certainty was uncommon and not necessarily unfavorable. In several cases, conventional interpretation classified MIBI-avid thyroid nodules as probable parathyroid adenomas; ultrasound correlation allowed these lesions to be recognized as typical intrathyroidal nodules rather than parathyroid pathology, appropriately lowering certainty or reclassifying the finding as negative. Thus, the intervention strategy primarily clarified initially uncertain or negative conventional interpretations and helped prevent false-positive overcalling of benign thyroid nodules, rather than merely increasing nonspecific positivity.

4.1. Conventional Workflow Optimization in the PET/CT Era

The present findings should be interpreted within the broader evolution of parathyroid imaging. Contemporary guidelines and recent studies increasingly emphasize hybrid SPECT/CT and PET/CT-based approaches, particularly F-18 fluorocholine PET/CT, for preoperative localization in primary hyperparathyroidism [2,3,6]. However, advanced

parathyroid imaging pathways are not uniformly available in routine practice and depend on scanner availability, radiopharmaceutical access, regulatory approval, reimbursement, local logistics, trained personnel, and cost.

This limitation is not restricted to low-resource settings. A global Nuclear Medicine Global Initiative survey identified supplier dependency, regulatory barriers, reimbursement issues, workforce limitations, and facility-related constraints as important determinants of access to nuclear medicine procedures [15]. Similarly, Canadian imaging inventory data show that stand-alone SPECT systems continue to operate alongside SPECT/CT units even in a high-income healthcare system [16]. Therefore, optimizing conventional scintigraphy workflows remains clinically relevant wherever access to hybrid SPECT/CT, PET/CT, or newer PET tracers is limited or inconsistent.

Conventional parathyroid scintigraphy should not be regarded as a fixed technique with uniform diagnostic value across centers. Its clinical utility depends on acquisition protocol, reader experience, image-processing strategy, and anatomical correlation. Prior studies have evaluated dual-tracer subtraction, computer-assisted analysis, pinhole or SPECT/CT-based approaches, combined scintigraphic techniques, and reader agreement in parathyroid scintigraphy [12,17–23]. A short-execution-time Tc-99m sestamibi/Tc-99m pertechnetate double-subtraction protocol has also been proposed as a low-cost alternative; however, its original two-stage processing requires generation of an intermediate thyroid image followed by a second subtraction, thereby adding processing complexity. The authors also described a mathematically equivalent single-step formulation [24]. However, most focused primarily on diagnostic accuracy, lesion detection, protocol comparison, or reader agreement. In contrast, the present study evaluated whether software-assisted subtraction, combined with ultrasound-correlated interpretation, improves reporting confidence, reduces ambiguity, and increases clinically actionable localization in a prospective reporting framework.

Accordingly, our findings should not be interpreted as suggesting equivalence to PET/CT or hybrid SPECT/CT. Rather, they indicate that when conventional scintigraphy remains the available first-line nuclear medicine method, software-assisted subtraction with targeted ultrasound correlation can serve as a pragmatic workflow optimization strategy.

4.2. Role of Ultrasound-Correlated Interpretation

Ultrasound correlation was a central component of the intervention strategy. Although cervical ultrasonography is widely available and provides high-resolution anatomical assessment of the thyroid bed and perithyroidal region, its performance is operator-dependent and may be affected by ectopic glands, small lesions, concomitant thyroid nodular disease, multiglandular disease, and prior neck surgery [7]. Therefore, ultrasound was not used as a stand-alone reference standard in this study, but as an anatomical correlation tool to support scintigraphic interpretation.

This distinction is important because conventional sestamibi imaging may show persistent or focal uptake without clearly defining its anatomical origin. Thyroid nodules may retain sestamibi and mimic parathyroid adenomas, whereas small parathyroid lesions may be obscured by adjacent thyroid activity. In such cases, subtraction imaging can improve lesion conspicuity, while ultrasound correlation can help determine whether the residual focus is intrathyroidal, extrathyroidal, lymph nodal, or anatomically compatible with a parathyroid lesion.

Our findings are consistent with previous studies supporting the complementary value of ultrasound and sestamibi-based imaging for preoperative localization [10,25]. The present study extends this concept into a reporting framework in which ultrasound-correlated interpretation was integrated with software-assisted subtraction to reduce am-

biguity in conventional scintigraphy reports. This integrated approach appeared useful not only for increasing confidence in true localization candidates, but also for reducing inappropriate confidence in misleading thyroidal uptake.

The exploratory ultrasound-related analyses should therefore be interpreted as describing the behavior of the integrated intervention strategy rather than as independent evidence of ultrasound performance. In this study, ultrasound is best understood as a complementary anatomical modifier of scintigraphic interpretation, not as an external comparator or independent diagnostic test.

4.3. Reference-Based Validation in the Operated Subgroup

The operated subgroup provided an opportunity to examine whether improved report actionability corresponded to reference-confirmed localization. Although this subgroup was limited in size and included only patients with surgical/pathological confirmation, the findings supported the clinical relevance of the reported results. INT showed higher PTA detection sensitivity than CTRL, although this difference did not reach statistical significance. More importantly, correct localization was significantly higher with INT, and there were no cases in which CTRL correctly localized the reference-confirmed lesion while INT failed to do so (Table 4).

This distinction is clinically important because parathyroid imaging is primarily used to guide surgical localization rather than simply to indicate whether a lesion may be present. A positive but incorrectly localized report may still misdirect operative planning. In the operated subgroup, the major advantage of the intervention strategy was therefore improved concordance between the reported lesion location and the surgical/pathological reference location.

The localization-level ROC analyses further characterized this effect by expanding each operated patient into six candidate parathyroid sites and evaluating whether each reporting strategy distinguished the reference-positive site from the remaining candidate sites. In this framework, INT demonstrated higher localization-level sensitivity while maintaining high specificity, resulting in higher binary operating-point and certainty-weighted AUC values than CTRL (Figure 8A,B). These findings support the interpretation that subtraction imaging, combined with ultrasound correlation, improved lesion localization rather than merely increasing nonspecific positive reporting.

These analyses should still be interpreted cautiously. The operated subgroup was not a full diagnostic-accuracy cohort because it consisted only of reference-positive patients who underwent surgery; therefore, patient-level specificity, negative predictive value, Youden index, and the classical disease-detection AUC could not be estimated. The localization-level analysis also included multiple candidate sites per patient and should be regarded as a descriptive assessment of localization discrimination rather than independent patient-level diagnostic accuracy. Accordingly, the reference-based findings should be viewed as supportive validation of the primary reporting endpoints, not as definitive evidence of diagnostic superiority.

4.4. Interpretation of PTH-Stratified and Lesion-Size Findings

The benefit of the intervention strategy was observed across clinically relevant PTH strata. As expected, both CTRL and INT endpoint-positive rates tended to be higher in patients with higher PTH levels, consistent with previous studies reporting an association between PTH level and sestamibi positivity or accurate localization, while smaller or lower-weight lesions are more likely to yield false-negative MIBI findings [26,27]. However, the relative advantage of INT over CTRL was maintained across the main PTH categories, and clinically actionable gain was not restricted to the highest PTH group. This is relevant

because patients with milder biochemical disease may have smaller or less conspicuous lesions, in whom conventional scintigraphy can be less definitive.

The exploratory lesion measurement analyses further support this interpretation. Previous studies have reported that MIBI-positive parathyroid adenomas tend to have larger volumes and higher iPTH levels than MIBI-negative adenomas [28]. In our cohort, however, lesion dimensions and estimated lesion volume were broadly comparable between patients with and without clinically actionable gain. Because lesion measurements were derived from INT reports, these analyses should be interpreted descriptively and not as independent predictors. Nevertheless, the absence of a clear size advantage among clinically gained patients suggests that the benefit of INT was not simply attributable to larger or more easily visible lesions.

Overall, the PTH-stratified and lesion-size findings suggest that software-assisted subtraction with ultrasound-correlated interpretation functioned as a confidence-enhancing strategy across a heterogeneous routine cohort, rather than merely improving interpretation in patients with advanced biochemical disease or large lesions.

4.5. Clinical Implications

The main clinical implication is that conventional parathyroid scintigraphy reports can be made more actionable by applying a structured interpretation strategy that combines software-assisted subtraction with targeted ultrasound correlation. In centers where hybrid SPECT/CT or F-18 fluorocholine PET/CT is not routinely available, conventional planar and SPECT imaging may remain the primary nuclear medicine approach for preoperative localization. In such settings, reducing equivocal or low-confidence interpretations may have immediate practical value.

The proposed workflow builds on commonly available components: Tc-99m pertechnetate thyroid imaging, dual-time-point Tc-99m sestamibi imaging, software-assisted subtraction, and high-resolution cervical ultrasound correlation. From a reporting perspective, its main advantage is the conversion of uncertain findings into more clinically interpretable localization statements that provide side- and pole-level localization, anatomical correlation, and diagnostic certainty. Such reports may be more useful for endocrine surgeons and multidisciplinary teams than nonspecific descriptions of possible persistent sestamibi uptake.

The approach may also help avoid overcalling thyroidal uptake as parathyroid pathology, particularly in patients with nodular thyroid disease. However, the present study did not assess surgical cure, operative time, conversion from focused to bilateral exploration, need for additional imaging, or cost-effectiveness. Therefore, the proposed workflow should currently be viewed as a pragmatic reporting optimization strategy rather than as a substitute for advanced hybrid or PET/CT-based imaging when those methods are available and clinically indicated.

4.6. Limitations

Several limitations should be considered when interpreting the present findings. First, this was a single-center preliminary study with a moderate sample size. Although the paired design reduced between-patient variability by allowing the same cases to be evaluated under two reporting conditions, the findings should be validated in larger, multicenter cohorts with different imaging systems, reader groups, and institutional workflows.

Second, the study was primarily designed to evaluate reporting confidence, interpretive certainty, and clinical actionability rather than definitive diagnostic accuracy. Surgical and histopathological confirmation was available only in a subset of patients, and the operated subgroup consisted only of reference-positive patients who underwent surgery. Therefore, patient-level specificity, negative predictive value, Youden index, and classical

disease-detection AUC could not be estimated. The localization-level ROC analysis partially addressed localization performance by evaluating candidate parathyroid sites within operated patients, but it remains exploratory and should not be interpreted as equivalent to patient-level diagnostic accuracy.

Third, ultrasound findings were incorporated into the INT interpretation workflow, and targeted correlation was performed by a single experienced operator. Because parathyroid lesions can be difficult to distinguish from thyroid nodules, lymph nodes, or other perithyroidal structures, operator- and expectation-related bias cannot be excluded, and interoperator reproducibility was not assessed. In addition, the specific LOGIQ P5 ultrasound unit available in our nuclear medicine department did not have an activated Doppler function. Consequently, color or power Doppler assessment of lesion vascularity could not be performed. Ultrasonography was therefore used primarily for targeted anatomical correlation with scintigraphic findings rather than as a comprehensive diagnostic neck ultrasound examination. Similarly, lesion dimensions and estimated lesion volume were derived from INT reports, and measurement-based analyses should be regarded as descriptive rather than independent predictors of clinical gain.

Fourth, both reporting arms were based on consensus interpretation by two-reader groups. This design reflects a controlled paired comparison of reporting strategies, but it does not allow assessment of individual reader variability or generalizability to less experienced readers. Future studies should evaluate interobserver agreement, reader-level performance, and reproducibility across different levels of expertise.

Finally, the study did not assess downstream clinical outcomes, including operative time, conversion from focused to bilateral exploration, cure rate, persistence or recurrence of hyperparathyroidism, need for additional imaging, or cost-effectiveness. Therefore, the present results should be interpreted as evidence that software-assisted subtraction with ultrasound-correlated interpretation improves reporting certainty and localization actionability, while further prospective outcome-based studies are required to define its impact on surgical management.

5. Conclusions

In this preliminary prospective reporting study, software-assisted subtraction imaging, combined with ultrasound-correlated interpretation, improved the clinical usability of conventional parathyroid scintigraphy. The intervention strategy increased reporting certainty, reduced ambiguous or non-actionable interpretations, and improved clinically actionable and high-confidence localization compared with conventional planar and SPECT-based interpretations.

In the operated subgroup, INT showed better concordance with surgical/pathological localization; however, these reference-based findings should be interpreted as supportive rather than definitive diagnostic accuracy evidence. As additional surgical/pathological reference data accumulate during follow-up, future analyses may allow more robust reference-based localization and ROC/AUC assessment. Overall, this workflow may represent a pragmatic optimization strategy for centers where hybrid SPECT/CT or PET/CT-based parathyroid imaging is not routinely available.

Supplementary Materials: The following supporting information can be downloaded at: https://www.mdpi.com/article/10.3390/diagnostics16152379/s1: Figure S1: Direction of change in reporting certainty after INT; Figure S2: Exploratory association between ultrasound-related findings and INT reporting endpoints; Figure S3: Estimated lesion volume (mm^3) according to clinical gain status; Table S1: Lesion location distribution and exploratory location-specific usefulness of the intervention strategy.

Author Contributions: S.B.: Conceptualization, Methodology, Investigation, Formal Analysis, Writing—Original Draft, Visualization. E.I.C.: Investigation, Data Curation, Formal Analysis. I.K.: Investigation, Data Curation, Validation. D.Y.: Investigation, Resources, Validation. K.K.: Investigation, Resources. O.O.G.: Investigation, Validation, Supervision. E.G.: Writing—Review and Editing, Supervision. E.A.: Writing—Review and Editing, Supervision. All authors have read and agreed to the published version of the manuscript.

Funding: This research received no external funding.

Institutional Review Board Statement: The study was conducted in accordance with the Declaration of Helsinki and approved by the Bursa Uludag University Ethics Research Committee (protocol code: 2025/7-15; approval date: 19 March 2025).

Informed Consent Statement: Informed consent was obtained from all subjects involved in the study.

Data Availability Statement: The data presented in this study are available on request from the corresponding author. The data are not publicly available due to patient privacy and ethical restrictions.

Conflicts of Interest: The authors declare no conflicts of interest.

References

1. Lalonde, M.N.; Correia, R.D.; Syktiotis, G.P.; Schaefer, N.; Matter, M.; Prior, J.O. Parathyroid Imaging. *Semin. Nucl. Med.* **2023**, *53*, 490–502. [CrossRef]
2. Boudousq, V.; Guignard, N.; Gilly, O.; Chambert, B.; Mamou, A.; Moranne, O.; Zemmour, M.; Sharara, H.; Lallemant, B. Diagnostic Performance of Cervical Ultrasound, (99m)Tc-Sestamibi Scintigraphy, and Contrast-Enhanced (18)F-Fluorocholine PET in Primary Hyperparathyroidism. *J. Nucl. Med.* **2022**, *63*, 1081–1086. [CrossRef]
3. Quak, E.; Lasne-Cardon, A.; Cavarec, M.; Lireux, B.; Bastit, V.; Roudaut, N.; Salaun, P.Y.; Keromnes, N.; Potard, G.; Vaduva, P.; et al. F18-Choline PET/CT or MIBI SPECT/CT in the Surgical Management of Primary Hyperparathyroidism: A Diagnostic Randomized Clinical Trial. *JAMA Otolaryngol. Head Neck Surg.* **2024**, *150*, 658–665. [CrossRef] [PubMed]
4. Kuyumcu, S.; Denizmen, D.; Has-Simsek, D.; Poyanli, A.; Uzum, A.K.; Buyukkaya, F.; Isik, E.G.; Onder, S.; Aksakal, N.; Ozkan, Z.G.; et al. (68)Ga-Trivehexin PET/CT: A promising novel tracer for primary hyperparathyroidism. *Eur. J. Nucl. Med. Mol. Imaging* **2024**, *51*, 3912–3923. [CrossRef] [PubMed]
5. Rep, S.; Sirca, K.; Lezaic, E.M.; Zaletel, K.; Hocevar, M.; Lezaic, L. [(18)F]fluorocholine PET vs. [(99m)Tc]sestamibi scintigraphy for detection and localization of hyperfunctioning parathyroid glands in patients with primary hyperparathyroidism: Outcomes and resource efficiency. *Radiol. Oncol.* **2024**, *58*, 486–493. [CrossRef] [PubMed]
6. Petranovic Ovcaricek, P.; Giovanella, L.; Carrio Gasset, I.; Hindie, E.; Huellner, M.W.; Luster, M.; Piccardo, A.; Weber, T.; Talbot, J.N.; Verburg, F.A. The EANM practice guidelines for parathyroid imaging. *Eur. J. Nucl. Med. Mol. Imaging* **2021**, *48*, 2801–2822. [CrossRef] [PubMed]
7. Centello, R.; Sesti, F.; Feola, T.; Sada, V.; Pandozzi, C.; Di Serafino, M.; Pacini, P.; Cantisani, V.; Giannetta, E.; Tarsitano, M.G. The Dark Side of Ultrasound Imaging in Parathyroid Disease. *J. Clin. Med.* **2023**, *12*, 2487. [CrossRef] [PubMed]
8. Michaud, L.; Balogova, S.; Burgess, A.; Ohnona, J.; Huchet, V.; Kerrou, K.; Lefevre, M.; Tassart, M.; Montravers, F.; Perie, S.; et al. A Pilot Comparison of 18F-fluorocholine PET/CT, Ultrasonography and 123I/99mTc-sestaMIBI Dual-Phase Dual-Isotope Scintigraphy in the Preoperative Localization of Hyperfunctioning Parathyroid Glands in Primary or Secondary Hyperparathyroidism: Influence of Thyroid Anomalies. *Medicine* **2015**, *94*, e1701. [CrossRef] [PubMed]
9. Morris, M.A.; Saboury, B.; Ahlman, M.; Malayeri, A.A.; Jones, E.C.; Chen, C.C.; Millo, C. Parathyroid Imaging: Past, Present, and Future. *Front. Endocrinol.* **2021**, *12*, 760419. [CrossRef] [PubMed]
10. Tawfik, A.I.; Kamr, W.H.; Mahmoud, W.; Abo Shady, I.A.; Mohamed, M.H. Added value of ultrasonography and Tc-99m MIBI SPECT/CT combined protocol in preoperative evaluation of parathyroid adenoma. *Eur. J. Radiol. Open* **2019**, *6*, 336–342. [CrossRef] [PubMed]
11. Kettle, A.G.; O'Doherty, M.J. Parathyroid imaging: How good is it and how should it be done? *Semin. Nucl. Med.* **2006**, *36*, 206–211. [CrossRef] [PubMed]
12. Krakauer, M.; Wieslander, B.; Myschetzky, P.S.; Lundstrom, A.; Bacher, T.; Sorensen, C.H.; Trolle, W.; Nygaard, B.; Bennedbaek, F.N. A Prospective Comparative Study of Parathyroid Dual-Phase Scintigraphy, Dual-Isotope Subtraction Scintigraphy, 4D-CT, and Ultrasonography in Primary Hyperparathyroidism. *Clin. Nucl. Med.* **2016**, *41*, 93–100. [CrossRef] [PubMed]
13. Huang, Z.; Lou, C. (99m)TcO(4)(-)/(99m)Tc-MIBI dual-tracer scintigraphy for preoperative localization of parathyroid adenomas. *J. Int. Med. Res.* **2019**, *47*, 836–845. [CrossRef] [PubMed]

14. Bilezikian, J.P.; Khan, A.A.; Silverberg, S.J.; Fuleihan, G.E.; Marcocci, C.; Minisola, S.; Perrier, N.; Sitges-Serra, A.; Thakker, R.V.; Guyatt, G.; et al. Evaluation and Management of Primary Hyperparathyroidism: Summary Statement and Guidelines from the Fifth International Workshop. *J. Bone Miner. Res.* **2022**, *37*, 2293–2314. [CrossRef] [PubMed]
15. Cutler, C.S.; Bailey, E.; Kumar, V.; Schwarz, S.W.; Bom, H.S.; Hatazawa, J.; Paez, D.; Orellana, P.; Louw, L.; Mut, F.; et al. Global Issues of Radiopharmaceutical Access and Availability: A Nuclear Medicine Global Initiative Project. *J. Nucl. Med.* **2021**, *62*, 422–430. [CrossRef] [PubMed]
16. Canadian Agency for Drugs and Technologies in Health. *Canadian Medical Imaging Inventory 2022–2023: SPECT and SPECT–CT: CMII Report*; Canadian Agency for Drugs and Technologies in Health: Ottawa, ON, Canada, 2024.
17. Carlier, T.; Oudoux, A.; Mirallie, E.; Seret, A.; Daumy, I.; Leux, C.; Bodet-Milin, C.; Kraeber-Bodere, F.; Ansquer, C. 99mTc-MIBI pinhole SPECT in primary hyperparathyroidism: Comparison with conventional SPECT, planar scintigraphy and ultrasonography. *Eur. J. Nucl. Med. Mol. Imaging* **2008**, *35*, 637–643. [CrossRef] [PubMed]
18. Vaz, A.; Griffiths, M. Parathyroid imaging and localization using SPECT/CT: Initial results. *J. Nucl. Med. Technol.* **2011**, *39*, 195–200. [CrossRef] [PubMed]
19. Dalar, C.; Ozdogan, O.; Durak, M.G.; Kocdor, M.A.; Bekis, R.; Cayvarli, H.; Kaya, G.C.; Comlekci, A.; Degirmenci, B. Interobserver and intraobserver agreement in parathyroid scintigraphy: How can parathyroid scintigraphy be made more reliable? *Endocr. Pract.* **2012**, *18*, 538–548. [CrossRef] [PubMed]
20. Kobylecka, M.I.; Bajera, A.; Fronczewska-Wieniawska, K.; Maczewska, J.; Plazinska, M.T.; Krolicki, L. Computer program for analysis of parathyroid scintigraphy examinations: Combination of dual-tracer (subtraction) and double phase single-tracer washout techniques. *Nucl. Med. Rev. Cent. East. Eur.* **2016**, *19*, 58–62. [CrossRef] [PubMed]
21. Sebikali, M.J.; Warwick, J.M.; Doruyter, A.G. Combined versus subtraction-only technique in parathyroid scintigraphy: Effect on scan interpretation. *Nucl. Med. Commun.* **2020**, *41*, 883–887. [CrossRef] [PubMed]
22. Christensen, J.W.; Krakauer, M. Added Value of Subtraction SPECT/CT in Dual-Isotope Parathyroid Scintigraphy. *Diagnostics* **2020**, *10*, 639. [CrossRef] [PubMed]
23. Tunninen, V.; Varjo, P.; Kauppinen, T.; Holm, A.; Eskola, H.; Seppanen, M. (99m)Tc-Sestamibi/(123)I Subtraction SPECT/CT in Parathyroid Scintigraphy: Is Additional Pinhole Imaging Useful? *Int. J. Mol. Imaging* **2017**, *2017*, 2712018. [CrossRef] [PubMed]
24. Chehade, F.; Kanj, A.; Ghafari, E.; Hammoud, N.; Fakhereddine, N.; Ghazzawi, A. Tc-99m-sestamibi/Tc-99m pertechnetate dual-tracer scintigraphy of parathyroid glands with double image subtraction: A dedicated short execution time protocol. *Imaging Med.* **2021**, *13*, 1–10.
25. Patel, C.N.; Salahudeen, H.M.; Lansdown, M.; Scarsbrook, A.F. Clinical utility of ultrasound and 99mTc sestamibi SPECT/CT for preoperative localization of parathyroid adenoma in patients with primary hyperparathyroidism. *Clin. Radiol.* **2010**, *65*, 278–287. [CrossRef] [PubMed]
26. Geysen, A.; Decallonne, B.; Vander Poorten, V.; Deroose, C.M.; Van Laere, K.; Goffin, K.; Jentjens, S. Influence of medication and PTH levels on detection of parathyroid adenomas with dual isotope parathyroid scintigraphy. *Am. J. Nucl. Med. Mol. Imaging* **2021**, *11*, 207–217. [PubMed]
27. Liu, Y.; Yang, L.; Xu, H.; Yang, Y.; Liang, Y.; Yang, A.; Tang, X.; Lei, S.; Christakis, I.; Jitpratoom, P.; et al. Analysis of false-positive and false-negative results in (99m)Tc-MIBI SPECT/CT parathyroid imaging. *Quant. Imaging Med. Surg.* **2023**, *13*, 8669–8680. [CrossRef] [PubMed]
28. Kong, S.H.; Kim, J.H.; Kim, S.W.; Shin, C.S. Radioactive Parathyroid Adenomas on Sestamibi Scans: Low Parathyroid Hormone Secretory Potential and Large Volume. *Endocrinol. Metab.* **2021**, *36*, 351–358. [CrossRef] [PubMed]

Disclaimer/Publisher's Note: The statements, opinions and data contained in all publications are solely those of the individual author(s) and contributor(s) and not of MDPI and/or the editor(s). MDPI and/or the editor(s) disclaim responsibility for any injury to people or property resulting from any ideas, methods, instructions or products referred to in the content.